JOURNAL OF APPLIED ELECTROCHEMISTRY 24 (1994) 1–7

A submerged impinging gas jet for corrosion and electrochemical studies

B. POULSON

International Research and Development Ltd, Fossway, Newcastle-upon-Tyne, NE6 2YD, Great Britain

Received 30 September 1992; revised 18 May 1993

A submerged impinging gas jet corrosion test is described which offers a number of advantages over flowing rig or rotating specimen approaches to examining the effects of fluid movement on corrosion. The mass transfer behaviour and flow structures are characterised and examples of its use presented.

1. Introduction

The effect of solution movement on electrochemical reactions or corrosion is usually examined by rotating the specimen as in the rotating disc or rotating cylinder electrodes, or using a rig in which the fluid is pumped through tubes, orifices, bends or other relevant geometries. The advantages and disadvantages of each approach has been reviewed [1]; both can be quite expensive.

Another much simpler approach, detailed by Brownsden and Bannister [2], was described in 1932. Their suggestion was to use a small diameter ($\sim$ 0.3 mm) low pressure (0.69 bar or 10 p.s.i.) submerged gas jet impinging at 45° onto a specimen 1.7 mm away. In this geometry the air jet expands and entrains water before it hits the surface. The suggestion was that such an arrangement could replace the conventional impinging jet test [3]. Despite being described by both Champion [4] and Evans [5], the submerged impinging gas jet has – to this author's knowledge – not been used. It is, of course, especially relevant to reproducing droplet impingement which can occur in two phase annular flow, where other less appropriate uncharacterized techniques have been used [6].

An impinging gas jet, at much higher gas pressures, is also relevant to heat exchangers and, in particular, under abnormal conditions in a liquid cooled nuclear reactor. In this situation the concern is that a leak leads to damage of adjoining tubes. Kennedy and Collier [7] presented an elegant study of the structure of such a submerged impinging gas jet (SIGJ), as shown schematically in Fig. 1.

However, what is needed to allow the geometry to be used quantitatively to examine the effect of flow on corrosion or electrochemical reactions is a knowledge of the mass transfer that the jet causes on the impacting surface. This paper describes just such a study and gives examples of its use in corrosion investigations. The low conductivity of thin films on the target surface potentially causing problems with electrochemical measurements is also discussed.

2. Experimental details

Copper disc specimens 25.4 mm in diameter and 1.4 mm thick were cut from a bar and polished to 600 grit. Other copper, carbon steel and type 316 stainless steel specimens were produced in a similar manner. Specimens were weighed and their thickness measured using a Moore and Wright digital micrometer with a 1 μm resolution. All experiments were performed in a PVDF cell with a capacity of 1 dm^3 shown schematically in Fig. 2. The jet to specimen distance was measured using a travelling microscope with a resolution of 25 μm. The gas flow (nitrogen or air) was controlled using calibrated pressure regulators or gauges. The tests were for selected times or were terminated when specimen penetration causes a leak and a conductivity sensor indicates failure. Selected specimens were metallographically mounted, polished and metal loss profiles determined.

All mass transfer measurements were performed by measuring the corrosion rate of copper specimens in a 0.1 N HCl solution containing 4 g dm^{-3} of ferric ions added as ferric chloride. Temperature was 20 ± 3° C. This technique has been tested [8] and used to measure mass transfer at bends [9] in single phase and high quality two phase annular flow [10].

The mass transfer coefficient, K (mm s^{-1}), is given by

$$K = \frac{CR \times \rho_{Cu} \times M_{Fe}}{3600 \times M_{Cu} \times \Delta C} \quad (1)$$

where CR is the corrosion rate of copper (mm h^{-1}), ρ_{Cu} is the density of copper (g cm^{-3}), M_{Fe} and M_{Cu} are the molecular weights of iron and copper, and ΔC the concentration of ferric ions (g cm^{-3}).

Details of the material/environments used in the corrosion tests are listed in Table 1. Flow visualization was performed by photographing the jet impacting a glass screen at various distances and gas jet pressures.

Conductivity measurements were performed using a 1 mm diameter nickel electrode insulated from the surrounding 10 mm diameter nickel electrode. A storage oscilloscope was available to monitor

0021-891X

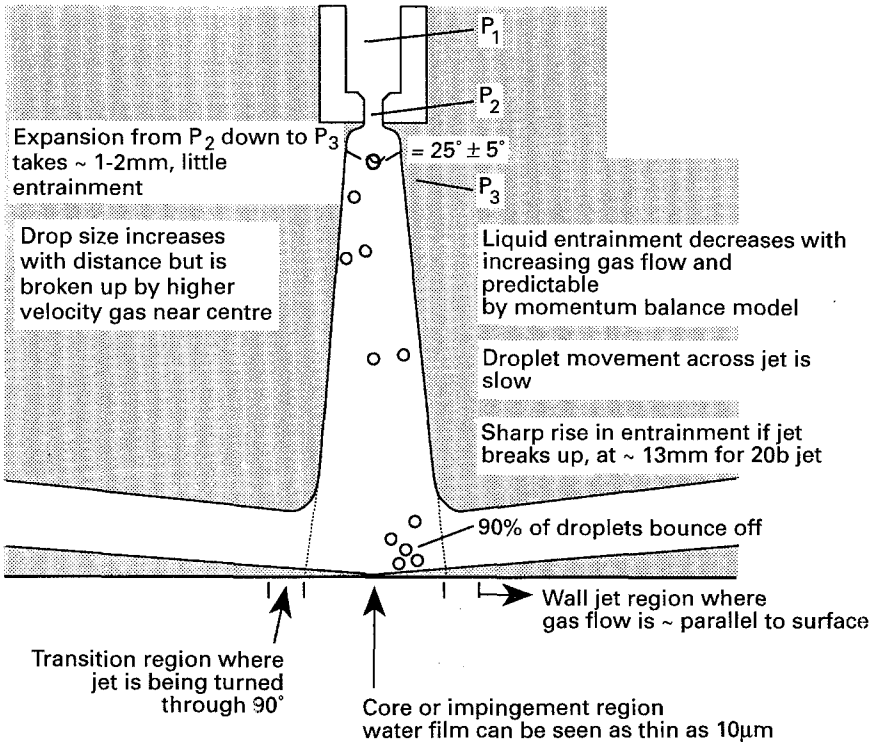

Fig. 1. Structure of submerged impinging gas jet (after Kennedy and Collier [7]).
Note: If $P_1(2/(\gamma+1))^{\gamma/\gamma+1} \geq P_3$ then nozzle is choked and the emerging gas is at the velocity of sound. For air or nitrogen the ratio of the molar heat capacities at constant pressure to that at constant volume (γ) is 1.4, so if P_3 is 1 bar the nozzle is choked if $P_1 > 1.9$ bar.

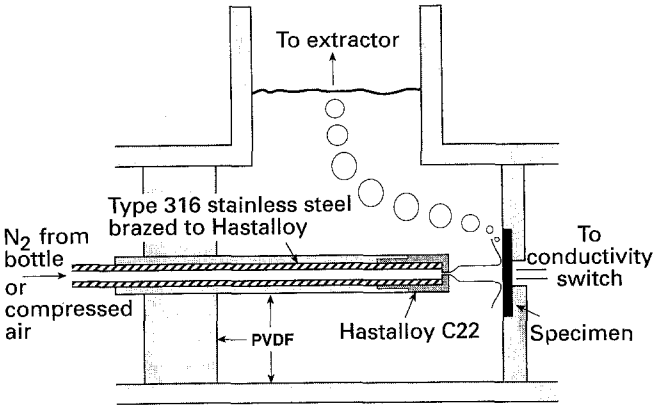

Fig. 2. Schematic diagram of submerged impinging gas jet cell.

'conductivity' with time in the hope of obtaining information about the structure of the impacted surface.

3. Results

Mass transfer measurements at different jet to specimen distances with a nitrogen gas pressure of 1 or 10 bar were performed. Typical specimen morphology is shown in Fig. 3. Particularly interesting is the lack of attack in the centre of the specimen tested at a jet-to-specimen distance of 1 mm. The maximum mass transfer coefficient measured in these tests, from time to leak data, is shown in Fig. 4. Typical mass transfer profiles across specimens determined from metallographic metal loss data are given in Fig. 5. The effect of gas jet pressure on the maximum K measured at a fixed jet to specimen distance of 5 mm are shown in Fig. 6. A limited number of tests were carried out at higher pressures up to 172 bar (2500 p.s.i.) without any additional increase in mass transfer coefficient being measurable.

Examples of flow visualization studies are shown in Fig. 7. These illustrate a number of features:

(i) The lack of any water entrainment at very low jet to specimen distances (Fig. 7(a)).

Table 1. Summary of corrosion tests

Material	*Environment*	*Summary*
Carbon steel	5 wt % HCl +0.2% armohib 28	Rapid corrosion at region of maximum mass transfer, due to inhibitor breakdown (see Fig. 8(c) and (d))
Type 316 stainless steel	Approx. 6 wt % $FeCl_3$	Pitting prevented but some dissolution at region of maximum K, transpassive dissolution? (see Fig. 8(b))
Copper	1 M $NaNO_2$	Very bright chemically polished region of maximum mass transfer surrounded by black Cu_2O. (see Fig. 8(e) and (f))

Conditions for all tests were: air at 7 bar at a jet to specimen distance of 5 mm with the environment at ambient temperature 20 ± 3° C, for 20 h.

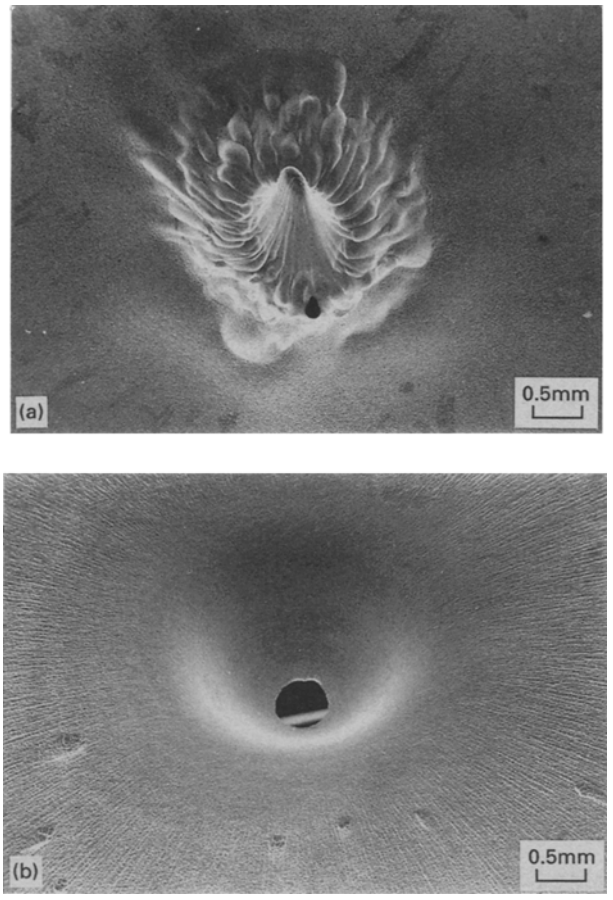

Fig. 3. Typical copper specimens used for mass transfer measurements. (a) 10 bar jet at height of 1 mm; (b) 10 bar jet at height of 10 mm.

(ii) The water entrainment limited to an outer annular ring at low jet to specimen distances (Fig. 7(b)).

(iii) As the jet to specimen distance is increased the region where entrained droplets impact the surface is enlarged (Fig. 7(b–d)).

(iv) As the jet to specimen distance increases further, the amount of entrained water increases and there is a gradual transition from gas containing entrained liquid droplets to predominantly liquid with gas bubbles (Fig. 7(e)).

(v) Finally at even greater jet to specimen distance buoyancy effects cause the gas bubbles to rise away from the horizontal axis of the cell eventually not reaching the target plate (Fig. 7(f)).

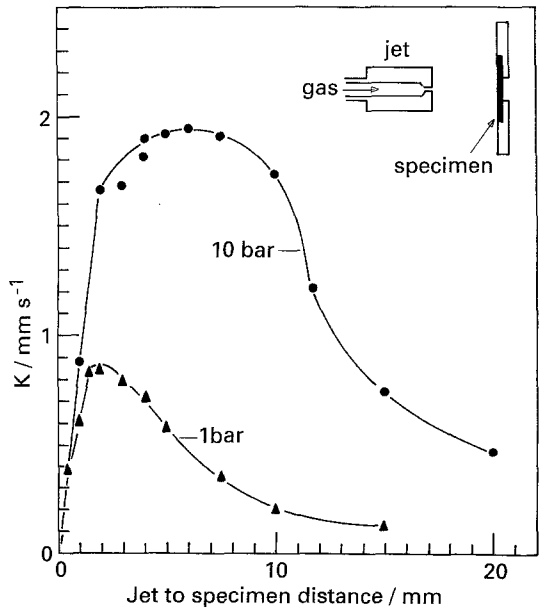

Fig. 4. Effect of jet to specimen distance on maximum mass transfer coefficient.

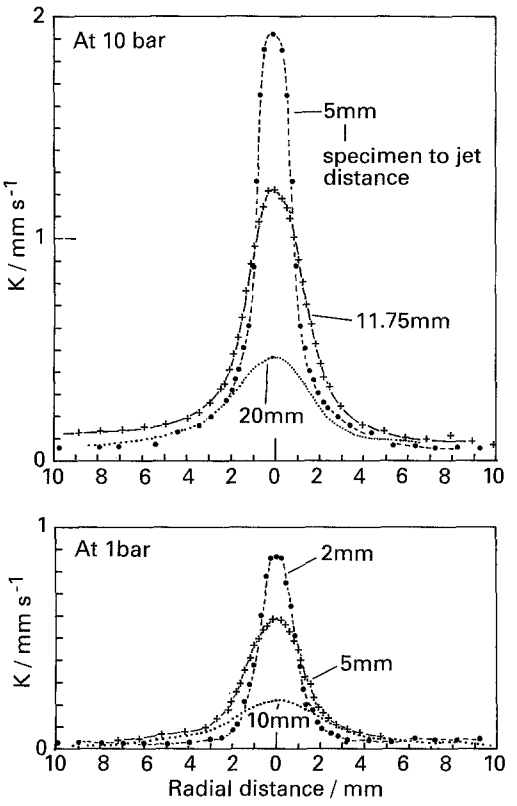

Fig. 5. Mass transfer coefficient profiles across representative samples.

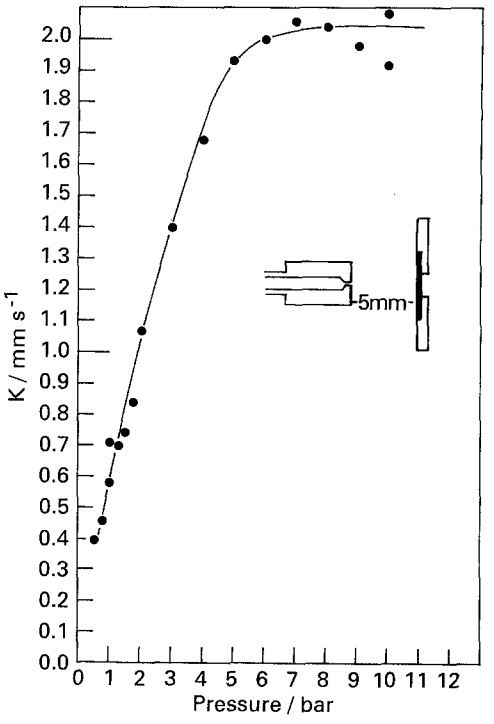

Fig. 6. Effect of gas pressure on maximum mass transfer coefficient at a jet to specimen distance of 5 mm.

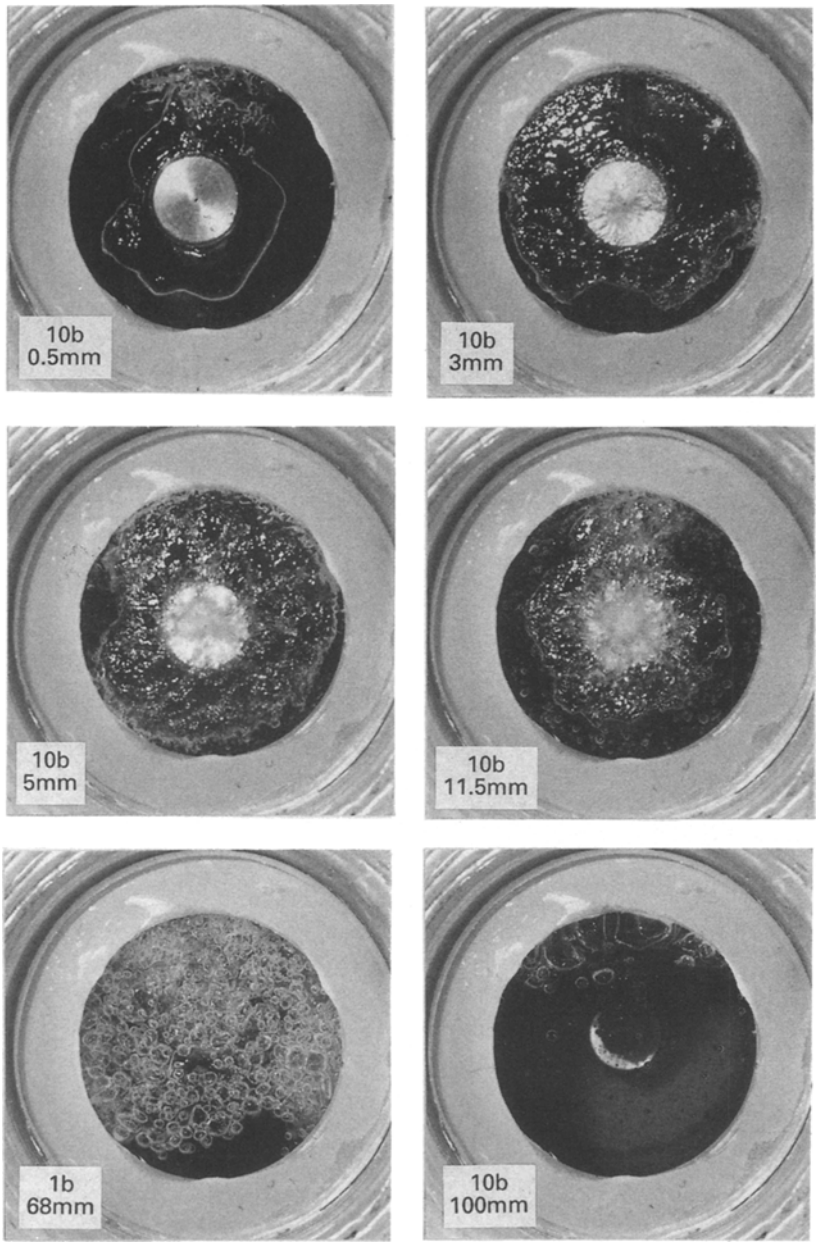

Fig. 7. Flow visualization: photographs of jet impacting a gas plate under various conditions.

The results of the corrosion tests are summarized in Table 1 with typical features being shown in Fig. 8. It must be emphasized that an air jet was used in these experiments and with the high rates of mass transfer of oxygen to the surface the attainment of high potentials might be possible.

When the conductivity measuring electrode is exposed to only liquid, its cell constant does not vary with time. However, under the impinging submerged gas jet and its associated two phase flow conditions, the cell constant rapidly varies reflecting the instantaneous flow conditions. From an examination of such traces it appears that six different flow regions can be differentiated:

(i) Very high cell constant; no liquid entrainment.
(ii) Very high cell constant with intermittent peaks reflecting intermittent entrainment (Fig. 9(d)).
(iii) High cell constant with relatively low amplitude variations; probably a thin continuous film continuously being replaced by the impact of droplets (Fig. 9(a)).
(iv) Lower cell constant with high amplitude variations suggesting a thicker liquid film being continuously disrupted by gas bubbles (Fig. 9(b) and (e)).
(v) Low cell constant which is occasionally increased as an air bubble impacts the surface (Fig. 9(c) and (f)).
(vi) Low stable cell constant.

Examples of these patterns are shown in Fig. 9 together with the time averaged cell constant at various gas pressures and jet to specimen distances.

4. Discussion

When a submerged gas jet impinges onto a specimen, the resultant mass transfer depends on the entrainment of liquid from the surrounding fluid and the

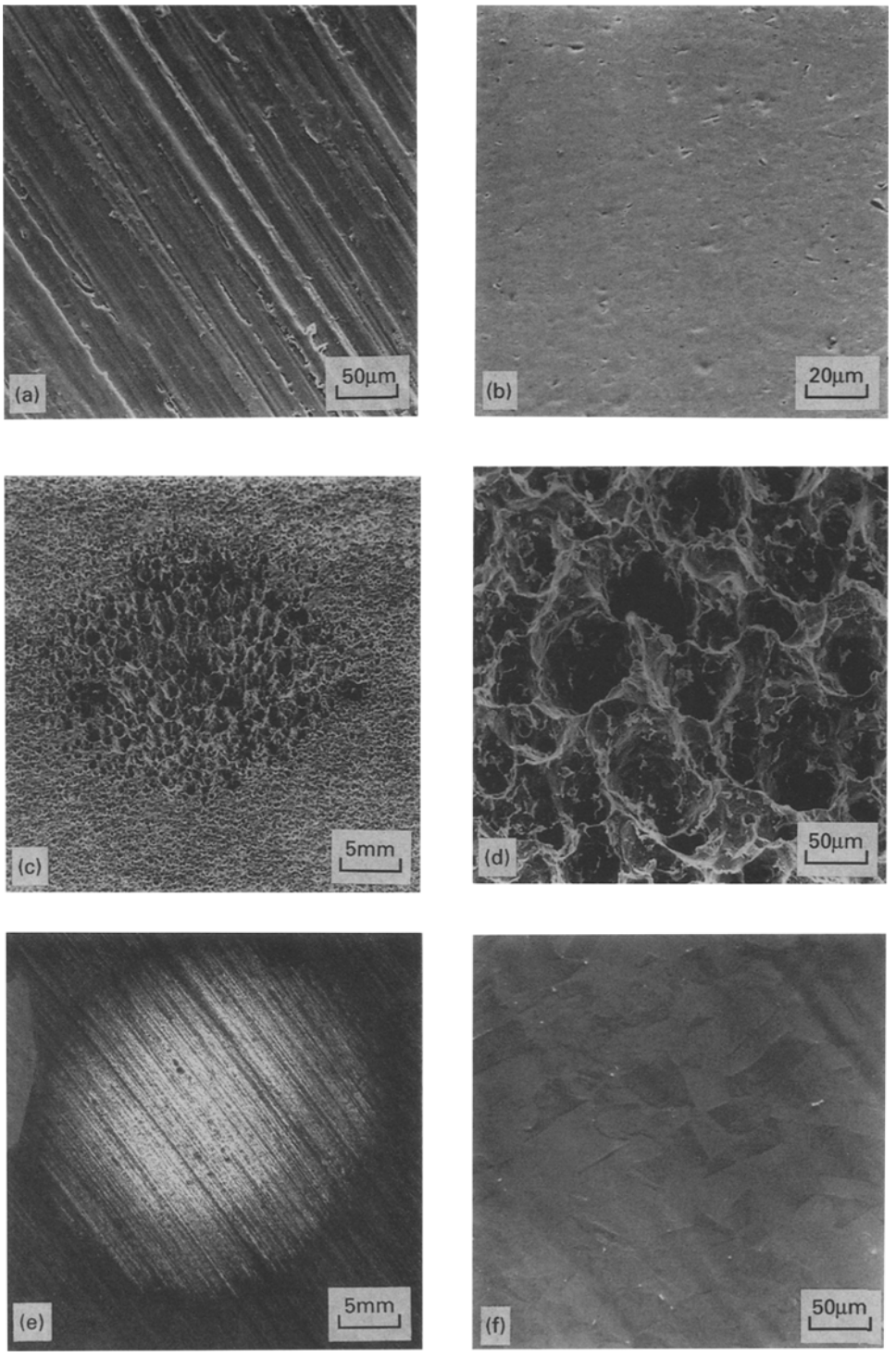

Fig. 8. Examples of using the submerged impinging gas jet in corrosion studies: (a) Typical untested surface; (b) type 316 in $FeCl_3$, high K region; (c) and (d) carbon steel in inhibited HCl; (e) and (f) copper in 1 M NO_2.

subsequent velocity that these drops impact the specimen. The shape of the mass transfer profile across individual specimens is thought to be more dependent on the gas velocity than the amount of entrained droplets once the latter is above some critical but low value. Thus at small jet to specimen distances the central region of the specimen remains unattacked (Fig. 3(a)), due to the absence of liquid. However, at greater jet to specimen distances the peak mass transfer rate is at the centre of the specimen, where the velocity will be highest although more liquid will be entrained at the perimeter of the jet.

The variation in maximum mass transfer coefficients at different jet-to-specimen distances, shown in Fig. 4, is also thought to result from these two competing processes of liquid entrainment which by momentum considerations reduces the gas plus droplet velocity. In addition, above a certain jet-to-specimen distance, the jet breaks up and the specimen then is exposed to bubble impact. These two flow regions are equivalent to annular flow and slug flow.

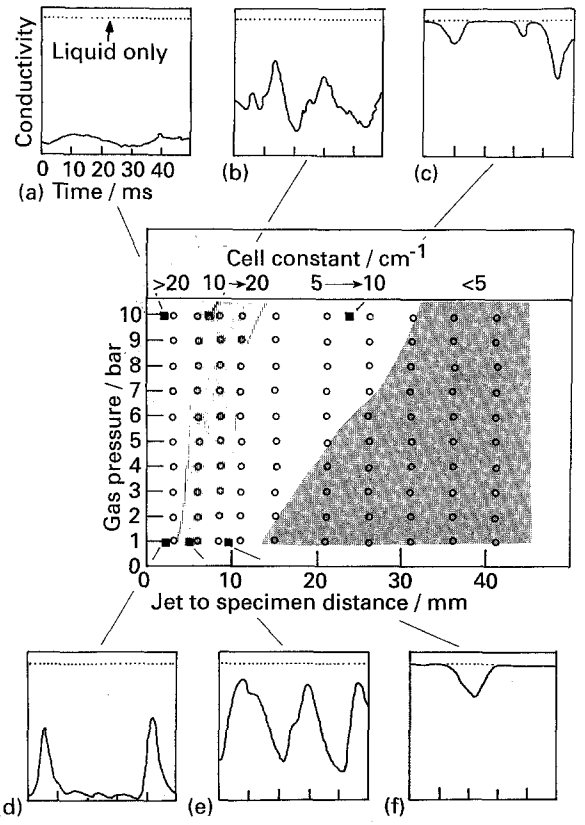

Fig. 9. Effect of jet to specimen distance and gas pressure on the effective cell constant and the conductivity variations with time.

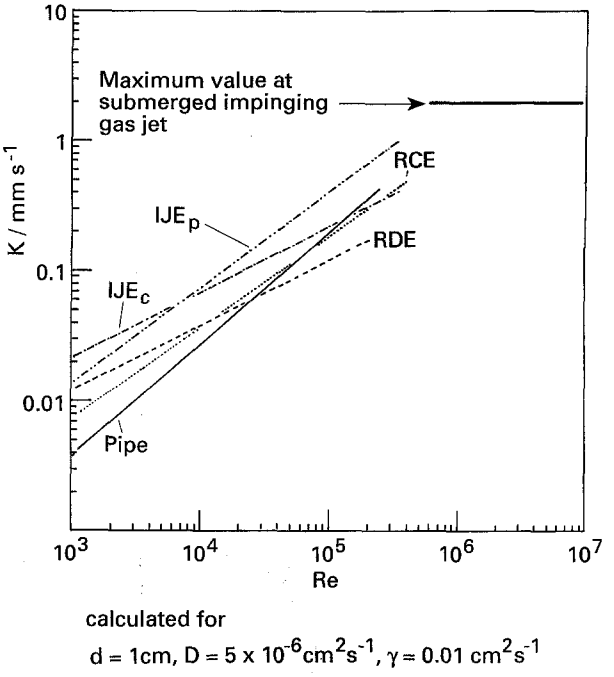

Fig. 10. Comparison of mass transfer coefficients for selected geometries compared to that obtainable with the submerged impinging gas jet. Legend: (– – –) RDE [14] $K = D/d \times 0.6205\, Re^{0.5} Sc^{0.33}$; (·····) RCE [15] $K = D/d \times 0.079\, Re^{0.7} Sc^{0.356}$; (– · – · –) IJE$_c$ [16] $K = D/d \times 1.12\, Re^{0.5} Sc^{0.33}$; (– · · · – · · · –) IJE$_p$ [17] $K = D/d \times 0.15\, Re^{0.73} Sc^{0.33}$; (———) pipe [13] $K = D/d \times 0.165\, Re^{0.86} Sc^{0.33}$. Values calculated for $d = 1$ cm, $D = 5 \times 10^{-6}$ cm^2 s^{-1}, $\gamma = 0.01$ cm^2 s^{-1}.

Perhaps not surprisingly the position and breadth of the region of maximum mass transfer occurs at increasing distances from the jet as the gas flow rate, which increases with gas pressure, increases.

The reason the maximum mass transfer appears to plateau at increasing gas pressures at a fixed jet to specimen distance of 5 mm is not known. It might be related to the exit gas velocity being limited to the speed of sound, and thermal cooling effects might become more important at higher gas flow rates.

Mass transfer data is usually presented as a correlation between the Sherwood number (*Sh*), the Reynolds number (*Re*) and the Schmidt number (*Sc*) of the form:

$$Sh = a\, Re^x\, Sc^y \qquad (2)$$

This is a neat expression but it can be misleading when comparing rates of mass transfer obtainable from different geometries. This is because, for a given geometry and environment, the mass transfer coefficient, K, is proportional to Re^x and d^{-1}. Of course in practice Re and d are not unrelated. For example if the diameter of a tube is decreased to increase K, this makes it more difficult to attain the same Re because of increased pressure drop requirements.

In Fig. 10 common specimen geometries are compared in terms of the K value achievable at a given value of Re for fixed values of d, D and γ; the maximum K that has been reported normalized to the given conditions is also indicated. It is clear that the SIGJ can generate mass transfer coefficients higher than those obtained with other geometries. It is remarkable that a 100 p.s.i. gas jet can generate K values higher than a 5.5 kW pump used to deliver 1.7 dm^3 s^{-1} through a 9.5 mm diameter impinging jet. The mass transfer coefficients recently measured at pipe bends in annular two phase flow [10] with superficial gas velocities up to 76 m s^{-1} are no higher than can be obtained using the SIGJ.

The problems using the SIGJ appear to be twofold. First, the small area of maximum mass transfer (Fig. 5) and large mass transfer gradients would make positioning of electrodes for electrochemical measurements critical; for corrosion studies this is not a problem. Secondly, the potential problem of high resistance to the passage of current that results from thin films on the surface. For very thin films there is a linear relationship between cell constant and film thickness [11]; the cell constant can be calculated from simple geometric considerations. The indications from this work is that films as thin as 10 μm can exist but under certain conditions they might be discontinuous. These observations are consistent with the earlier work of Kennedy and Collier [7]. Time averaged cell constants at various gas pressures and jet to specimen distances are shown in Fig. 9. This shows that for the electrode geometry employed the cell constant increases from a single phase value of 3.9 cm^{-1} to over 30 cm^{-1} at low jet to specimen distances and higher gas pressures. Whether this is a problem depends on the type of electrochemical measurements to be performed and the current

requirement. For example impedance measurements have been used successfully to monitor corrosion under thin films relevant to dew point corrosion [12], and have the advantage of readily assessing the resistive component [12].

5. Conclusions

1. The mass transfer characteristics of a submerged impinging gas jet electrode have been described. Such an arrangement allows the generation of very high rates of mass transfer very simply and cheaply compared to rotating or flowing systems. It thus offers considerable advantages for corrosion or electrochemical measurements.
2. Some examples of the use of a submerged impinging gas jet in corrosion investigations have been described including: (i) the effect of solution flow on pit initiation of 316 stainless steel; (ii) corrosion of copper in sodium nitrite solution; and (iii) the effect of flow on inhibitor breakdown in hydrochloric acid.
3. Preliminary investigations on the problems of performing electrochemical measurements due to the high resistance of the thin films in the impingement zone have been undertaken and 'effective' cell constants at various jet to specimen distances and gas pressures have been measured.

References

[1] B. Poulson, *Corros. Sci.* **23** (1983) 391.
[2] H. W. Brownsden and L. C. Bannister, *J. Inst. Metals* **49** (1932) 123.
[3] R. May, *J. Inst. Metals* **40** (1928) 14.
[4] F. A. Champion, 'Corrosion Testing Procedures', Chapman and Hall, London (1952) p. 134.
[5] U. R. Evans, 'The Corrosion and Oxidation of Metals', Edward Arnold, London (1960) p. 810.
[6] J. H. Gerretson, 'Inhibitor performance under liquid droplet impingement conditions in CO_2 containing environments'. Paper 254 presented at the International Conference on Advances in Corrosion and Protection, UMIST Manchester 28 June–3 July 1992.
[7] T. D. A. Kennedy and J. G. Collier, *I.Chem.E. Symp. Series 38*, I.Chem.E. Services, London (1974).
[8] B. Poulson and R. Robinson, *Corros. Sci.* **26** (1986) 265.
[9] *Idem*, *Int. J. Heat & Mass Transfer* **31** (1988) 1289.
[10] B. Poulson, *Chem. Eng. Sci.* **46** (1991) 1069.
[11] M. W. E. Coney, *J. Phys. E* **6** (1973) 903.
[12] W. M. Cox, D. M. Farrel and J. L. Dawson, 'Corrosion monitoring for process control' *in* 'Dewpoint Corrosion' (edited by D. R. Holmes), Ellis Horwood, Chichester (1985) pp. 191–217.
[13] F. P. Berger and K. F. F. L. Hue, *Int. J. Heat & Mass Transfer* **20** (1977) 1185.
[14] V. Levich, 'Physiochemical Hydrodynamics', Prentice Hall, New Jersey (1962).
[15] M. Eisenberg, C. W. Tobias and C. R. Wilkin, *J. Electrochem. Soc.* **101** (1954) 306.
[16] D. T. Chin and C. H. Tsang, *ibid.* **125** (1978) 1461.
[17] B. Poulson, 'Advances in understanding hydrodynamic effects on corrosion'. Paper 291 presented at the International Conference on Advances in Corrosion and Protection, UMIST, Manchester, 28 June–3 July 1992.
[18] B. Poulson, *Corros. Sci.* **30** (1990) 743.